Chapter-3

$KTaO_3$ based perovskites to develop superior Oxide-ion Electrolytes for SOFCs

3.1 Introduction

As described in chapter 1, novel ferroelectric-based materials, $Na_{0.5}Bi_{0.5}Ti_{1-x}Mg_xO_{3-\delta,}$ were explored to develop superior oxide-ion electrolytes.[1-3] Keeping this in background, we have utilized this novel concept of using the large polarizability of high κ dielectric materials to develop an oxide-ion electrolyte as the induced directive nature of polarization can accelerate the oxide-ion vacancy motion within the percolation limit. To realize this novel concept, we have investigated a $KTaO_3$ (a well-known ferroelectric)-based[4-5] perovskite structured material as a host to develop superior oxide-ion electrolytes. Cations with relatively smaller sizes, such as Ti^{4+} and $Ge^{4+,}$ were substituted on a Ta-site in the $KTaO_3$ structure to create the oxide-ion vacancy. The vibration of a smaller-sized Ti^{4+} cation from its mean position in octahedral coordination is already known to be the reason behind the high dielectric constant and ferroelectric transition in PZT-based ferroelectric ceramics. Here, we report the synthesis and characterization of Ti^{4+} and Ge^{4+} substituted $KTaO_3$.

3.2 Material Synthesis & Characterization

$KTa_{1-x-y}Ti_xGe_yO_{3-\delta}$ and $KTa_{1-x}M_xO_{3-\delta}$ (M = Ti and Ge) samples were synthesized using a solid-state reaction by mixing a stoichiometric amount of K_2CO_3, Ta_2O_5, TiO_2, and GeO_2 powder followed by heating at 900 °C for 12 h. Multiple heating cycles were carried out to make the single-phase material. Samples were heated three times at 900 °C for 15 h with intermediate grinding of the sample. For conductivity measurement, the powder was made into pellets of 10 mm diameter and ~0.2−0.25 cm thickness by pressing it with a 7−8 ton weight on a hydraulic press. These pellets were fired at 900 °C for 10 h for densification. The pellet density was measured using the Archimedes method, and it was found to be ~97% of the theoretical density of the material. The phase formation was studied through a Rigaku Miniflex desktop X-ray diffractometer (XRD) with Cu Kα radiation (λ = 1.54 Å) in the range

2θ ~ 10−90° with a step size of 0.02°. The structures were refined by the Rietveld refinement method using the FULLPROF suite software package and cubic $KTaO_3$ (space group:Pm3m) as a model structure. The sintered samples' microstructures were investigated using scanning electron microscopy (EVO, scanning electron microscope MA15/18). The average grain size was calculated using the linear intercept method. The composition of the compounds was examined by energy-dispersive X-ray (EDX) spectroscopy with a probe attached to the SEM instrument. The sintered pellets were coated with silver paste and cured at 500 °C for 30 min. Platinum wire was used as a contact for corrent collector. The conductivity measurements were performed using an Autolab potentiostat as a function of frequency from 1 Hz to 1 MHz at different temperatures varying from 100 to 650°C. All measurements were taken during the cooling cycle from 650 to 100°C.

3.3 Thermal study

I have tried to substitute up to 40% Ti or Ge and 60% Ti and Ge co-substitution in the $KTaO_3$ lattice. The synthesized Ti^{4+} and Ge^{4+} substituted $KTaO_3$ powder was white in colour. However, the material seems to be a little bit hygroscopic in nature. Therefore, thermogravimetric analysis (TGA) was carried out in an N_2 atmosphere from room temperature (25°C) to 900°C to study the weight loss due to water/moisture absorption and desorption of the materials. Figure 3.1 shows the TGA plot for the $KTa_{0.4}Ti_{0.3}Ge_{0.3}O_{3-\delta}$ sample preheated at 200°C. Up to 75°C, a negligible weight loss confirmed the sample's absence of physically absorbed water. However, there is a continuous weight loss (~0.5%) up to 200°C, a weight loss (~1.8%) up to 500°C, and very little or negligible loss detected above 500°C. The TGA study confirms the relatively low hygroscopic nature of the materials and the absence of absorbed moisture in the sample above 500°C.

Further, an FT-IR study was carried out to study the hydroxide formation, or water absorption on the surface of the Ti and Ge substituted $KTaO_3$ sample. Figure 3.2 shows comparison of

the FT-IR spectra of the $KTa_{0.4}Ti_{0.3}Ge_{0.3}O_{2.7}$ sample preheated at 200°C for 2 h and preheated at 500°C for 2 hours. The absence of peaks between 3300 and 4000 cm^{-1} clearly reveals the absence or negligible presence of hydroxide-ions or physio absorbed water on the sample.

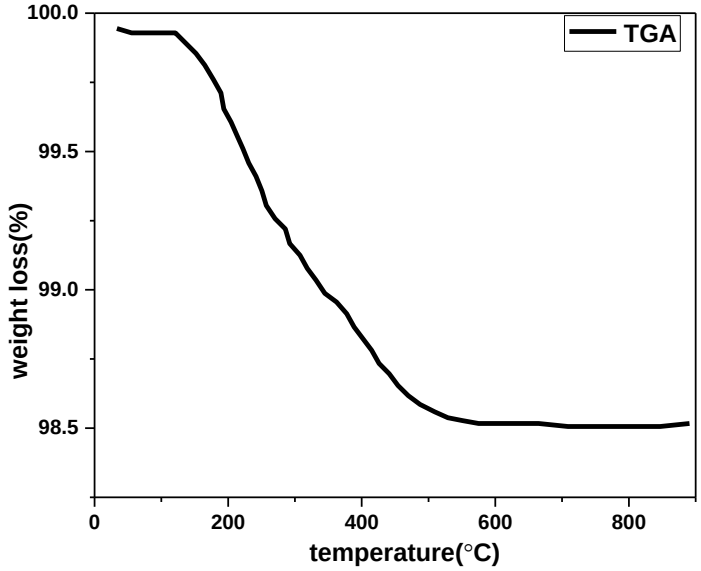

Figure 3.1 Thermogravimetric analysis (TGA) curve of $KTa_{0.4}Ti_{0.3}Ge_{0.3}O_{2.7}$

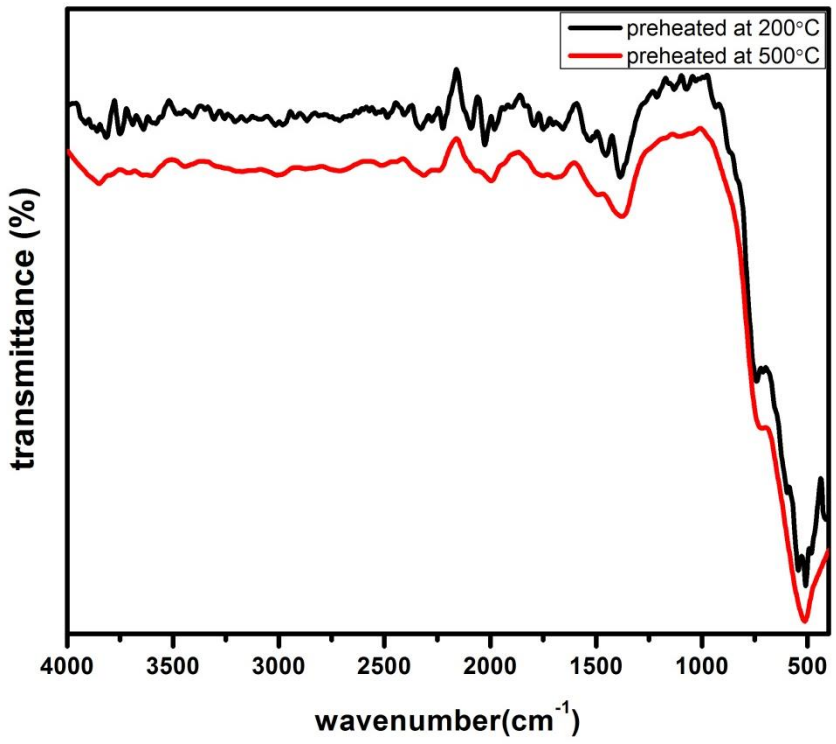

Figure 3.2 FT-IR spectra of $KTa_{0.4}Ti_{0.3}Ge0.3O_{2.7}$

3.4 Crystal Structure Study

The crystal structure and phase purity of the material were studied by powder XRD. The powder XRD patterns of $KTa_{0.6}Ti_{0.4}O_{2.8}$, $KTa_{0.6}Ge_{0.4}O_{2.8}$, and $KTa_{0.4}Ti_{0.3}Ge_{0.3}O_{2.7}$ are shown in Figure 3.3(a−c), respectively. All the peaks were identified as a $KTaO_3$ structure (JCPDS: 98-006-0322). Thus, single-phase $KTa_{0.6}Ti_{0.4}O_{2.8}$, $KTa_{0.6}Ge_{0.4}O_{2.8}$, and $KTa_{0.4}Ti_{0.3}Ge_{0.3}O_{2.7}$ were synthesized using a solid-state ceramic synthesis route with multiple heating at 900 °C for 15h. Crystal structures of Ti and Ge substituted $KTaO_3$ were refined using the Rietveld method. Figure 3.4 shows the Rietveld refined XRD profile of (a) $KTa_{0.6}Ti_{0.4}O_{3-0.5}$, (b) $KTa_{0.6}Ge_{0.4}O_{3-0.5x}$, and (c) $KTa_{0.4}Ti_{0.3}Ge_{0.3}O_{2.7}$. The fitted profile matched well with the observed XRD pattern. A small hump was obtained close to 28° in the XRD plot (Figures 3.3b and 3.4b). This may be due to the presence of small unreacted Ta_2O_5 phases in the material. Simultaneously, the Ti and Ge substituted perovskite sample does not show the presence of any traces of impurities or unreacted materials. The structural parameters obtained from Reitveld refinement of the powder XRD pattern are given in Table 3.1. The substitution of Ti^{4+} and Ge^{4+} on the Ta-site in the $KTaO_3$ lattice did not result in much of a change in the lattice parameter.[6] This may be due to the rigid nature of the octahedral network in the 3D structure of the perovskite lattice, along with the formation of oxide-ion vacancies.

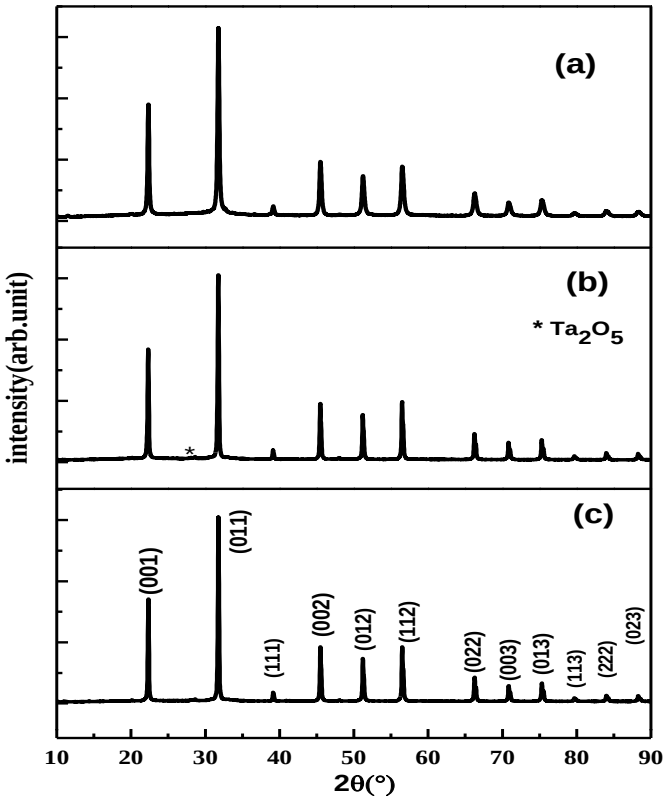

Figure 3.3 Powder XRD pattern (a) $KTa_{0.6}Ti_{0.4}O_{2.8}$ (b) $KTa_{0.6}Ge_{0.4}O_{2.8}$ and (c) $KTa_{0.4}Ti_{0.3}Ge0.3O_{2.7}$

Table 3.1: Structural parameter of Ta and Ge doped $KTaO_3$

Compound	**Lattice parameter(Å) (a=b=c)**	χ^2	R_f	R_{Bragg}
$KTaO_3$	*3.9920 (1) Ref. 8*	-	-	-
$KTa_{0.6}Ti_{0.4}O_{3-0.5x}$	3.9891(2)	3.39	5.137	6.490
$KTa_{0.6}Ge_{0.4}O_{3-0.5x}$	3.9887(1)	3.07	4.962	7.493
$KTa_{0.4}Ti_{0.3}Ge_{0.3}O_{2.7}$	3.9899(2)	0.88	1.295	2.713

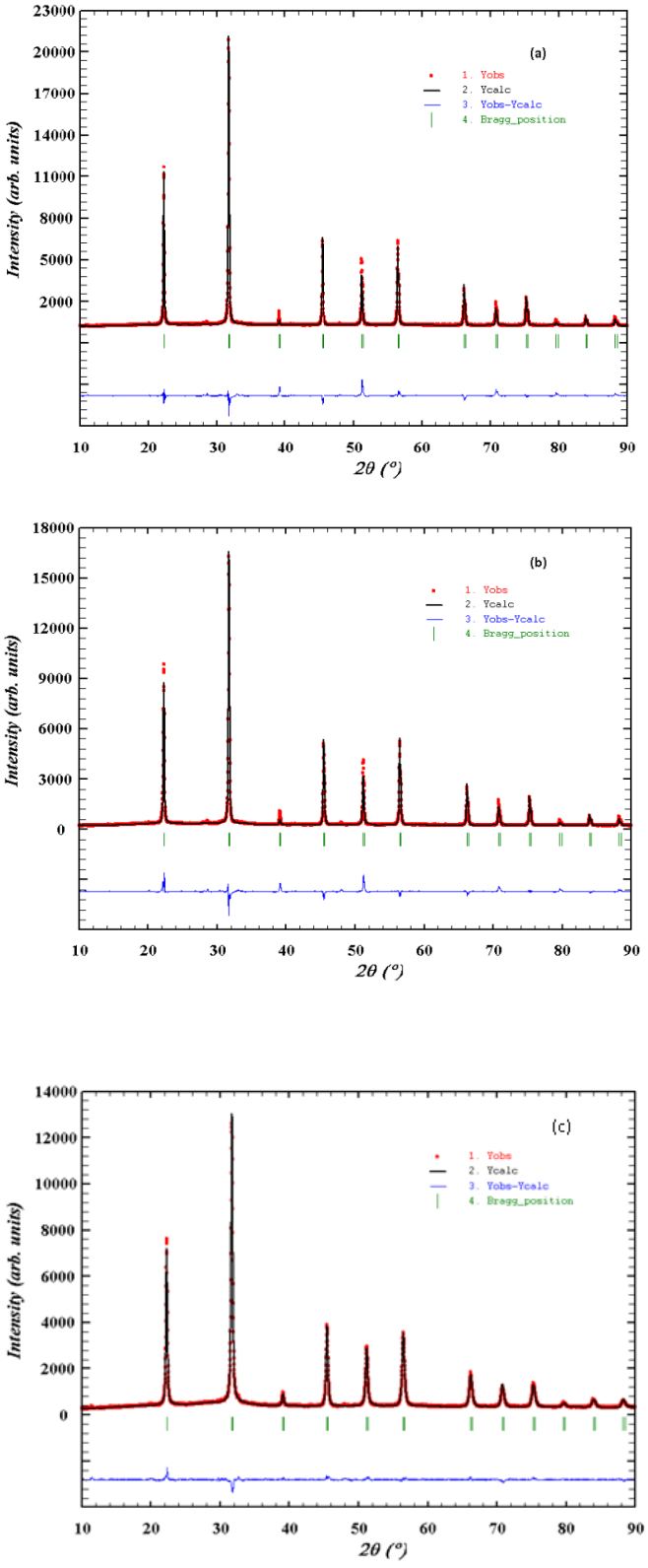

Figure 3.4 Rietveld refined powder XRD profile of (a) $KTa_{0.6}Ti_{0.4}O_{2.8}$ (b) $KTa_{0.6}Ge_{0.4}O_{2.8}$ and (c) $KTa_{0.4}Ti_{0.3}Ge0.3O_{2.7}$

3.5 SEM/EDAX Study

SEM micrographs of $KTa_{0.4}Ti_{0.3}Ge_{0.3}O_{2.7}$ (powder, front view and cross-section of the pellet utilized for conductivity measurement) are given in Figure 3.5(a−c). The SEM study reveals that the powder sample is 4−10µm in size. Figure 3.5(b,c) also shows the images of the front and cross-section of the pellet. The microstructure of the pellets has almost no or very low porosity, and the grains are interconnected (in good contact with each other) due to crystal growth during sintering. The EDX study (micrograph shown in Figure 3.5d) also confirms that the composition of the materials is close to the nominal composition taken for the synthesis of the material.

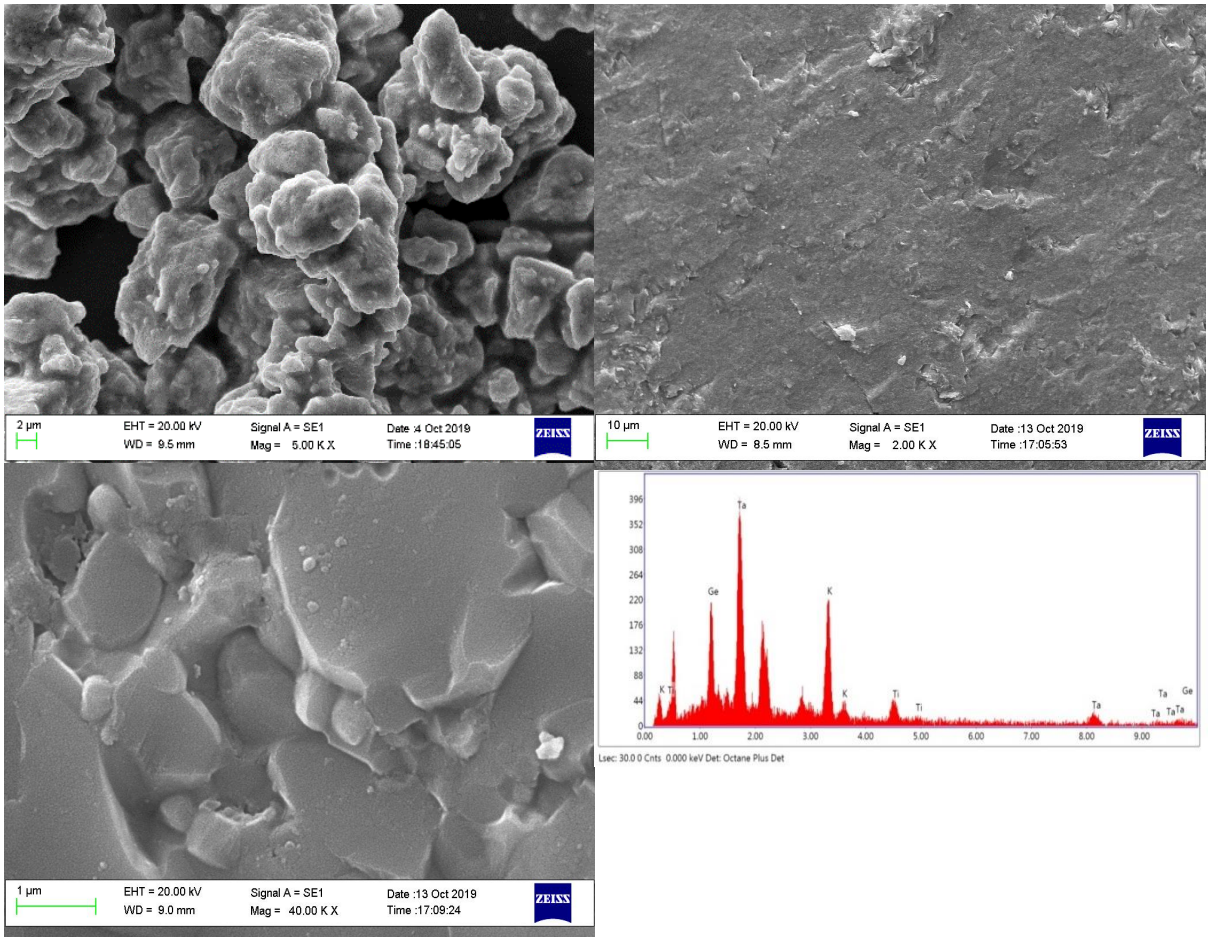

Figure 3.5 SEM image $KTa_{0.4}Ti_{0.3}Ge0.3O_{2.7}$ (a) Powder (b) Front view of the pellet (c) Cross-section of the pellets and (d) image of EDX spectra

3.6 EIS Study

The oxide-ion conductivity study was carried out using impedance spectroscopy at various temperatures in different environments. Figure 3.6(a) shows the oxide-ion conductivity for different composition of Ti and Ge substituted $KTaO_3$, i.e., (i) $KTa_{0.6}Ti_{0.4}O_{2.8}$, (ii) $KTa_{0.6}Ge_{0.4}O_{2.8}$, and (iii) $KTa_{0.4}Ti_{0.3}Ge_{0.3}O_{2.7}$. Only Ti and Ge substituted $KTaO_3$ have shown low oxide-ion conductivity; however, oxide-ion conductivity was continuously increasing with increasing temperature for $KaTa_{0.6}Ti_{0.4}O_{2.8}$ and $KTa_{0.6}Ge_{0.4}O_{2.8}$. The best oxide-ion conductivity of this series was observed for the composition $KTa_{0.4}Ti_{0.3}Ge_{0.3}O_{2.7}$. At 550°C, the measured oxide-ion conductivity was $\sim 10^{-2}$ S cm^{-1}, which is equivalent to the oxide-ion conductivity of $La_{0.8}Sr_{0.2}Ga_{0.83}Mg_{0.17}O_3$ (LSGM) at 600°C and of $Zr_{0.92}Y_{0.08}O_2$ (YSZ) around 700°C. A sudden increase in oxide-ion conductivity around 400°C was observed in the case of all samples. This may be due to the percolation limit of the oxygen vacancy migration in connection with a dielectric relaxation related phase transition at elevated temperatures. However, further advanced phase transition studies such as neutron powder diffraction (NPD) or EXAFS studies are important to reveal the phase transition and associated dielectric relaxation or transition. The conductivity of $KTa_{0.4}Ti_{0.3}Ge_{0.3}O_{2.7}$ was also measured in hydrogen (UHP H_2) and nitrogen (UHP N_2) environments (Figure 3.6b) to see the effect of the absorbed moisture, hydrogen, and oxygen on the surface of the sample. Below 500°C, the total conductivity of $KTa_{0.4}Ti_{0.3}Ge_{0.3}O_{2.7}$ was lower in hydrogen and nitrogen atmospheres than in air. This may be because some absorbed moisture or hydroxide-ions present in the sample can contribute to the additional protonic type conductivity at lower temperatures. We have also compared the measured oxide-ion conductivity of $KTa_{0.4}Ti_{0.3}Ge_{0.3}O_{2.7}$ in the same temperature range (300−650°C) with those of other established oxide-ion conductors having crystal structures of fluorite or perovskite (Figure 3.6c). Oxide-ion conductivity of $KTa_{0.4}Ti_{0.3}Ge_{0.3}O_{2.7}$ is very comparable to Sr- and Ga-doped $LaGaO_3$, LSGM. The data for

oxide-ion conductivity of different samples of $KTa_{1-x-y}Ti_xGe_yO_{3-\delta}$ at different temperatures and the data of other competitive oxide-ion electrolytes in the same temperature range are given in Table 3.2. The activation energy for oxide-ion conductivity was found to be as low as 0.34 eV. The Cole-Cole plot at 600 °C for $KTa_{0.4}Ti_{0.3}Ge_{0.3}O_{2.7}$ is shown to understand the polarisation and the oxide-ion transport nature (Figure 3.7). The inset of Figure 3.7 shows the impedance data between 33 kHz and 20 Hz.

To study the effect of dielectric polarizability on oxide-ion conductivity, the dielectric constant at various temperatures in the frequency range of 20−100 kHz is plotted in Figure 3.8. The dielectric studies show a diffusive phase transition characterized by a strong temperature and frequency dependence of the permittivity and relaxor behaviour. The highest dielectric constant was found for ~5300 at 20 kHz at 650°C. The T_m was varying or decreasing with increasing applied frequency. This linear decrease confirms the relaxor nature of the high dielectric behaviour of $KTa_{0.4}Ti_{0.3}Ge_{0.3}O_{2.7}$. However, in the case of a regular relaxor dielectric, T_m increases linearly with the applied frequencies. Thus, our study confirms the relaxation of the dipole moment that can contribute to the high oxide-ion conductivity of the material. The relaxation of the net dipole moment generated over oxygen vacant octahedral can reorient the polyhedra at an elevated temperature to provide the short transportation or pathways for the oxide-ion vacancy migration. The high leakage in dielectric permittivity due to Bi deficiency and oxygen vacancies induced during materials processing is also related to high oxide-ion conduction is also reported for $Na_{0.5}Bi_{0.5}TiO_3$-based samples.[1] Similarly, the relationship between oxide-ion conduction and dielectric relaxation was also reported for 20% Sm-doped CeO_2 ($Ce_{0.8}Sm_{0.2}O_{2-\delta}$).[7] However, further studies are necessary to confirm the relationship between high dielectricity and the dielectric relaxation with oxide-ion conductivity of the material. Our study can guide the development of superior oxide-ion electrolytes using the novel high κ dielectric and ferroelectric materials.

Table 3.2 O^{2-} conductivity (σ) of $KTa_{1-x-y}Ti_xGe_yO_{3-\alpha}$ at different temperatures

	Conductivity ($S.cm^{-1}$)			
Compound	***650°C***	**600°C**	**550°C**	**500°C**
$KTa_{0.6}Ti_{0.4}O_{3-0.5x}$	$1.2x10^{-3}$	$6.6x10^{-4}$	$4.3x10^{-4}$	$1.6x10^{-4}$
$KTa_{0.6}Ge_{0.4}O_{3-0.5x}$	$8.3x10^{-4}$	$5.3x10^{-4}$	$2.9x10^{-4}$	$1.1x10^{-4}$
$KTa_{0.4}Ti_{0.3}Ge_{0.3}O_{2.7}$	$5.2x10^{-2}$	$3.1x10^{-2}$	$9.8x10^{-3}$	$8.5x10^{-3}$
$Na_{0.5}Bi_{0.49}Ti_{0.98}Mg_{0.02}O_{2.965}$ [1]		$6.6x10^{-3}$	$5.4x10^{-3}$	$3.5x10^{-3}$
$Zr_{0.92}Y_{0.08}O_{1.96}$ [1]		$4.4x10^{-3}$	$2.3x10^{-3}$	$1x10^{-3}$
$Ce_{0.9}Gd_{0.1}O_{1.95}$ [1]		$2.3x10^{-2}$	$1.2x10^{-2}$	$6.5x10^{-3}$
$La_{0.9}Sr_{0.1}Ga_{0.9}Mg_{0.1}O_{2.9}$ [1]		$2.5x10^{-2}$	$1.5x10^{-2}$	$6.5x10^{-3}$

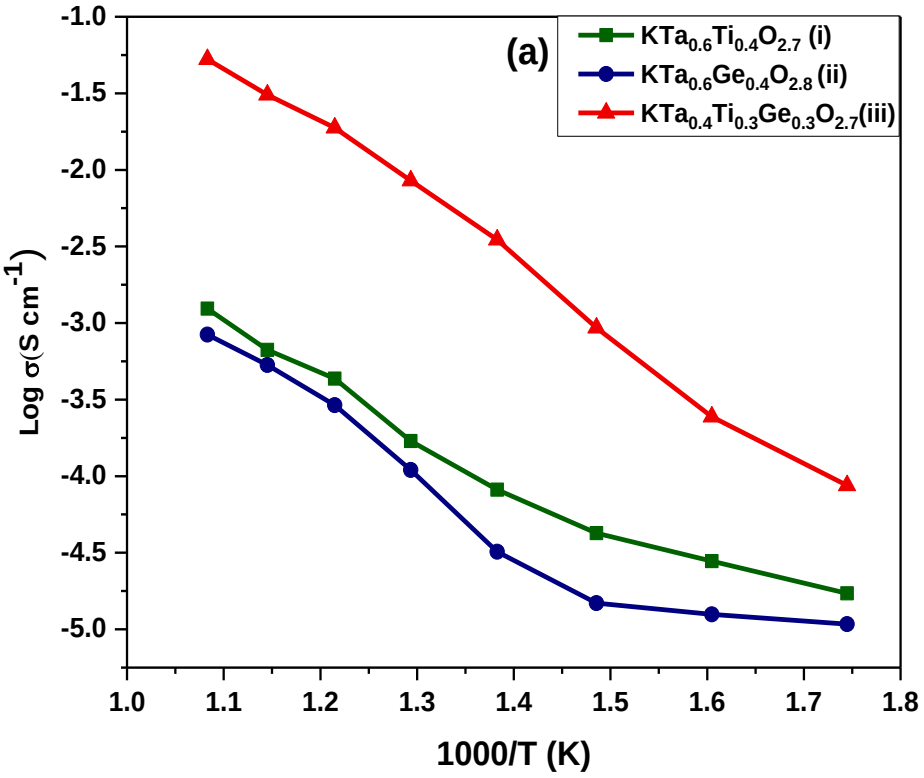

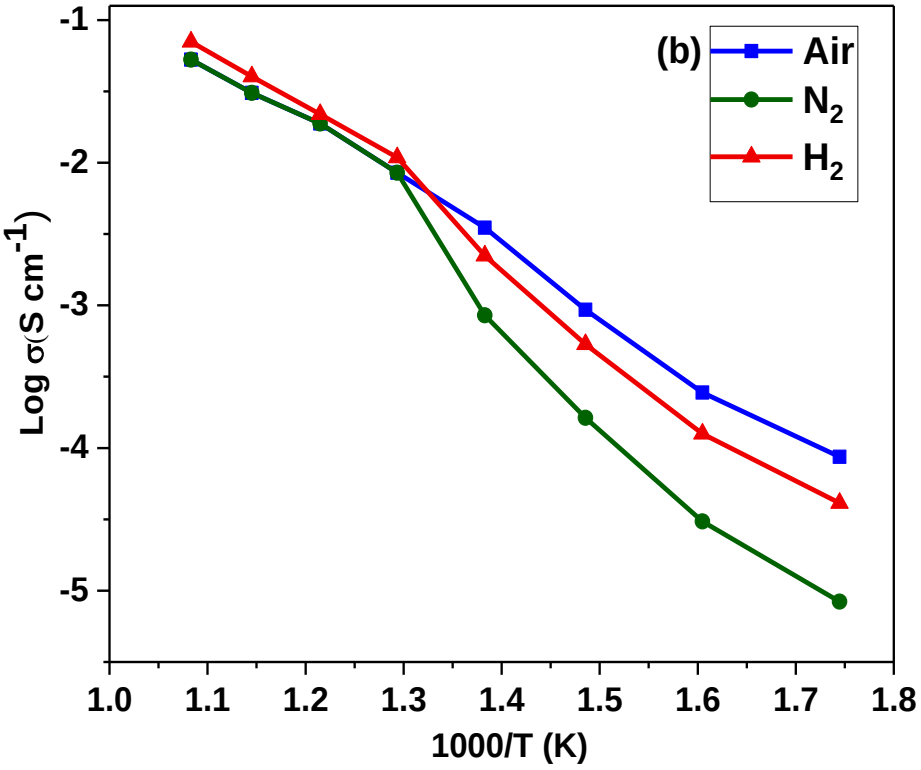

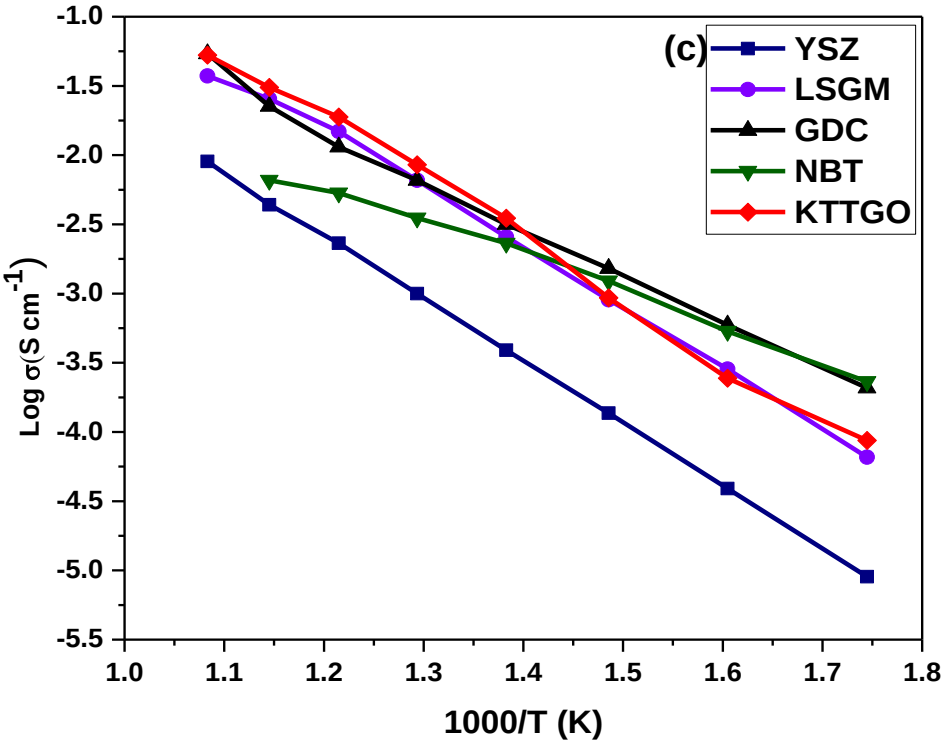

Figure 3.6. Arrhenius plot of (a) various compositions, (b) $KTa_{0.4}Ti_{0.3}Ge0.3O_{2.7}$ in different mediums, (c) comparison of existing intermediate temperature Oxide-ion electrolytes in the air from Ref. 1.

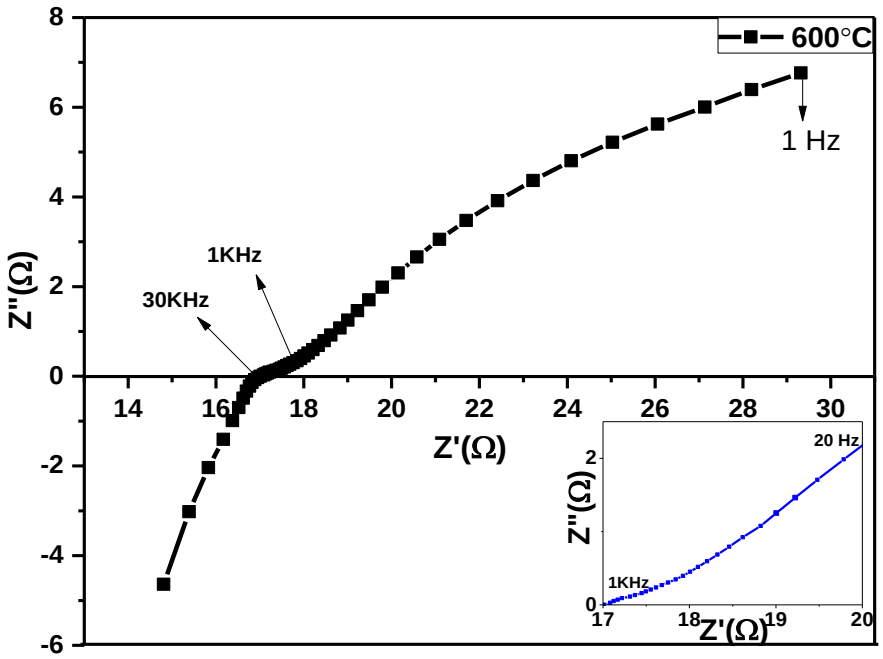

Figure 3.7 Cole-Cole plot of $KTa_{0.4}Ti_{0.3}Ge_{0.3}O_{2.7}$ at 600 ^{o}C. Inset shows the plot between 30 kHz to 20Hz frequencies.

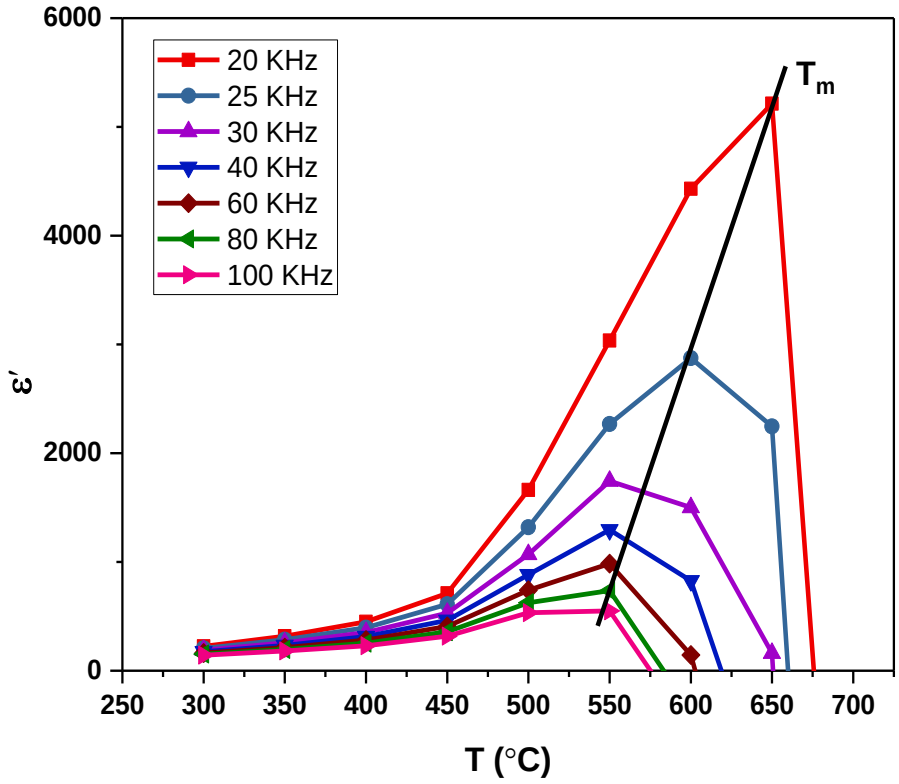

Figure 3.8. The dielectric constant of $KTa_{0.4}Ti_{0.3}Ge_{0.3}O_{2.7}$ at different temperatures and frequencies.

3.7 CONCLUSION

We have substituted up to 40% Ti or Ge and 60% Ti and Ge co-substitution in the $KTaO_3$ lattice. The material has been characterized as an electrolyte for IT-SOFCs using various characterization techniques such as powder XRD, SEM-EDX, and impedance spectroscopy. Few of the samples were purely in the phase shown in this chapter, while others had impurities. Among all $KTa_{0.4}Ti_{0.3}Ge_{0.3}O_{2.7}$ samples showed superior oxide-ion conductivity with the lowest activation energy within the temperature range 300−650°C. The oxide-ion conductivity of $KTa_{0.4}Ti_{0.3}Ge_{0.3}O_{2.7}$ was found 10^{-2} s/cm close to 550°C. Owing to the simple formulation/preparation/processing coupled with high oxide-ion conductivity at intermediate temperatures (500−650°C), the materials can be a potential candidate as an oxide-ion electrolyte for intermediate temperature solid oxide fuel cells (IT-SOFCs). However, further studies are necessary to see the applicability of the materials as an oxide-ion electrolyte for the development of IT-SOFCs.